Three-dimensional structure of the diphtheria toxin repressor in complex with divalent cation co-repressors

Xiayang Qiu[1], Christophe LMJ Verlinde[1], Suping Zhang[2], Michael P Schmitt[2], Randall K Holmes[2] and Wim GJ Hol[1]*

[1]Department of Biological Structure, Biomolecular Structure Program, and Howard Hughes Medical Institute, SL-15, School of Medicine, University of Washington, Seattle, WA 98195, USA and [2]Department of Microbiology and Immunology, Uniformed Services, University of the Health Sciences, Bethesda, MD 20814, USA

Background: When *Corynebacterium diphtheriae* encounters an environment with a low concentration of iron ions, it initiates the synthesis of several virulence factors, including diphtheria toxin. The diphtheria toxin repressor (DtxR) plays a key role in this iron-dependent, global regulatory system and is the prototype for a new family of iron-dependent repressor proteins in Gram-positive bacteria. This study aimed to increase understanding of the general regulatory principles of cation binding to DtxR.

Results: The crystal structure of dimeric DtxR holorepressor in complex with different transition metals shows that each subunit comprises an amino-terminal DNA-binding domain, an interface domain (which contains two metal-binding sites) and a third, very flexible carboxy-terminal domain. Each DNA-binding domain contains a helix-turn-helix motif and has a topology which is very similar to catabolite gene activator protein (CAP). Molecular modeling suggests that bound DNA adopts a bent conformation with helices α3 of DtxR interacting with the major grooves. The two metal-binding sites lie ~10 Å apart. Binding site 2 is positioned at a potential hinge region between the DNA-binding and interface domains. Residues 98–108 appear to be crucial for the functioning of the repressor; these provide four of the ligands of the two metal-binding sites and three residues at the other side of the helix which are at the heart of the dimer interface.

Conclusions: The crystal structure of the DtxR holorepressor suggests that the divalent cation co-repressor controls motions of the DNA-binding domain. In this way the metal co-repressor governs the distance between operator recognition elements in the two subunits and, consequently, DNA recognition.

Structure 15 January 1995, **3**:87–100

Key words: *Corynebacterium diphtheriae*, diphtheria toxin, iron-dependent repressor, siderophores, *tox* gene

Introduction

Iron is essential in virtually all living organisms for a wide variety of cellular processes. Hence, sophisticated mechanisms have evolved to obtain sufficient amounts of this important cation. The solubility of ferric ions in water at neutral pH is extremely low, ~10^{-18} M. In body fluids of humans and animals, iron is solubilized and transported by proteins such as transferrin and lactoferrin, which bind iron very tightly. Most pathogenic bacteria have developed mechanisms by which they can take up iron ions when present within human or animal hosts. One method used is the synthesis and secretion of siderophores, low-molecular mass chelators with high affinity for iron. The bacteria utilize special uptake systems to assimilate the iron from these ferri-siderophore complexes.

Although the low concentration of iron in the human host prevents attack by certain bacteria, many pathogens use this low iron concentration as a signal for both induction of iron-uptake systems and as a signal for the production of other virulence factors, such as toxins (for a review, see [1]). Such regulation is controlled by iron-dependent repressors, such as Fur (the ferric uptake regulation protein in several Gram-negative bacteria) and the diphtheria toxin repressor (DtxR) from *Corynebacterium diphtheriae*.

DtxR, encoded by *C. diphtheriae*, is a 25 kDa protein that consists of 226 residues [2–17]. *In vitro*, oxidation of DtxR by atmospheric oxygen causes the gradual formation of stable but inactive dimers [9]. It is likely that dimerization is the result of a disulfide cross-link between the single cysteine residue in each of the two monomers, as full activity can be restored by reducing agents [9]. In the living cell, however, a low redox potential is present, and the functioning of the repressor is determined by the properties of the reduced, non-cross-linked form of the protein.

DtxR is activated by a variety of divalent cations — the physiologically relevant one being Fe(II). As long as the intracellular concentration of Fe(II) in *C. diphtheriae* is sufficiently high, DtxR coordinately represses a family of genes that encode diphtheria toxin, components of the high-affinity iron-uptake system, and possibly other virulence-associated proteins. Specific targets of the holorepressor include the *tox*, *irp1* and *irp2* operators (Fig. 1) [5,7,13]. DNase I footprinting and hydroxyl-radical protection experiments demonstrated that the repressor binds to a region ~30 bp long comprising a conserved 19 bp central region that is moderately AT-rich, and non-conserved ends that vary greatly in base composition [9,13–15]. Changes of DNA sequence at specific positions within the operator lead to loss of repressor binding

*Corresponding author.

 ISSN 0969-2126

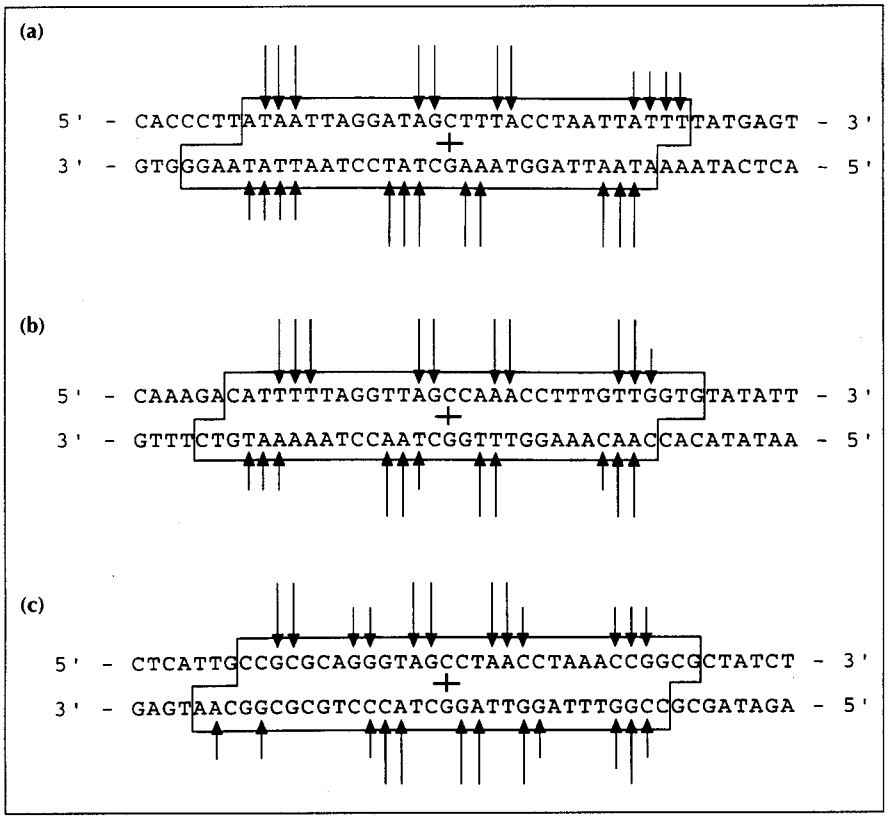

Fig. 1. Results of DNA footprinting experiments with the **(a)** *tox,* **(b)** *irp1* and **(c)** *irp2* operators [13]. The top sequence is the coding strand. The boxes indicate the region protected from DNase I cleavage by bound DtxR. The arrows indicate nucleotides protected from hydroxyl radical cleavage by DtxR; long arrows indicate strong protection, short arrows weak protection. The cross at the center of each sequence shows the dyad of the pseudo-palindrome.

[8,9], indicating the great selectivity of the repressor for its operator. Analysis of amino acid substitutions in mutant forms of DtxR that resulted in loss of repressor activity, combined with recognition of sequence similarities between DtxR and other dimeric DNA-binding proteins such as catabolite gene activator protein (CAP), λ repressor and Cro repressor, led to the proposal that residues 28–49 of DtxR form a helix-turn-helix DNA-binding motif that functions in recognition of DtxR-regulated operators [6,10,12,16].

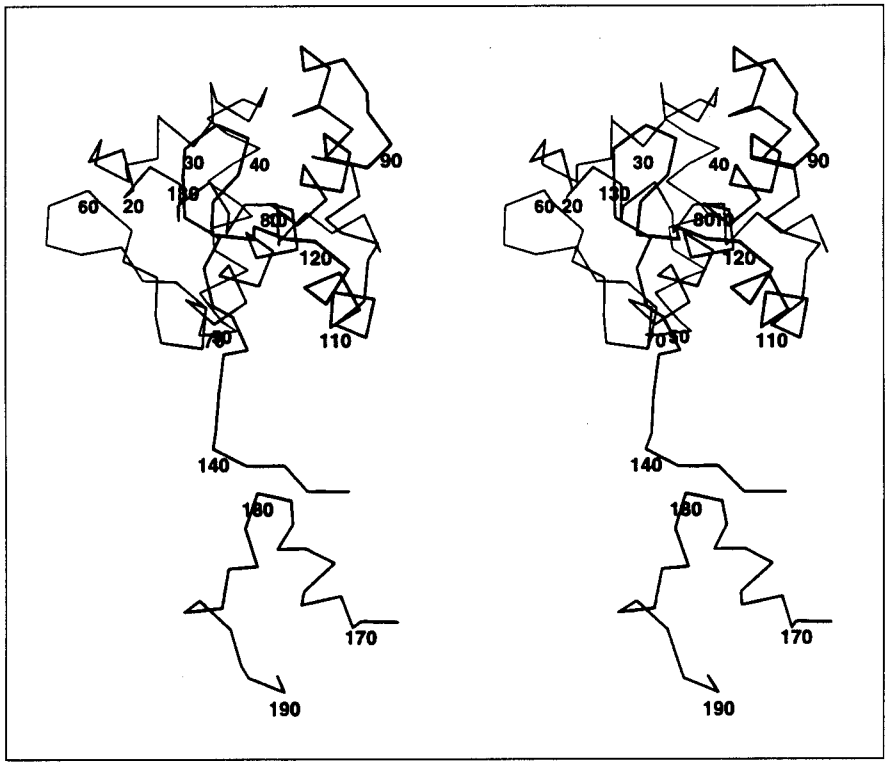

Fig. 2. Stereo figure of the C^{α} chain in a single subunit of DtxR. No electron density is observed for residues 1–3, 145–167 and 192–226, and these are therefore not depicted. The secondary-structure elements of DtxR identified so far are as follows: helix α1 consists of residues 7–21; helix α2, 27–33; helix α3, 38–50; strand β1, 54–56; strand β2, 62–64; helix α4, 66–88; helix α5, 94–104; helix α6, 110–117 and helix α7, 172–175.

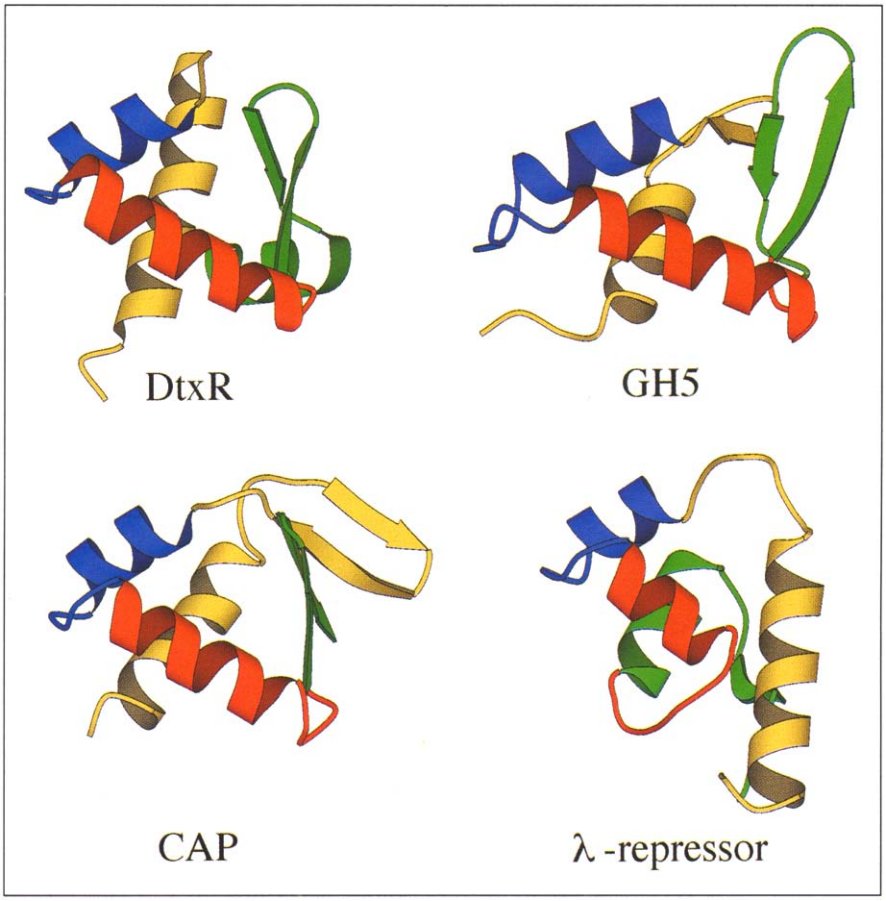

Fig.3. Comparison of DNA-binding domains. In each structure, helix α1 is shown in yellow, helix α2 in blue and helix α3 in red. The residues following α3 are shown in green. Note how in the λ repressor helix α4 occupies approximately the same position as (here green) helix α1 in the other DNA-binding domains depicted. (Drawn using MOLSCRIPT [33].)

The activity of DtxR as a function of cation type and concentration has been the subject of several investigations. When the cation concentration drops below a certain threshold, into the micromolar range in the case of Fe(II), the repressor loses its divalent cationic co-repressor and the resultant apo-repressor is unable to bind to the operators. Although Fe(II) is potent in activating the repressor *in vivo* [1], Ni(II), Fe(II), Mn(II), Co(II), Zn(II) and Cd(II) are all able to activate DtxR *in vitro* [12,14]. Zn(II) is slightly less effective as an activator than the other cations. Cu(II) fails to promote the formation of the DtxR–tox complex [12,14]. Each subunit possesses one high-affinity metal-ion-binding site [16], and, it has recently emerged, a second binding site of lower affinity (Z Wang, MP Schmitt and RK Holmes, unpublished data).

The importance of residue Cys102 to repressor activity was investigated by saturation mutagenesis studies [12]. Only the Cys102→Asp mutant retained partial activity whereas all other 18 amino acid substitutions for Cys102 abolished DtxR repressor activity. The authors concluded that, given the frequent involvement of sulfhydryl groups in cation binding, Cys102 resides in the metal-binding site of DtxR. Wang *et al.* [16] have recently reported several other mutants with impaired metal-binding properties, and concluded that the region 98–106 is important for metal coordination. This region contains not only the sulfhydryl of Cys102 but also other potential transition metal ion ligands such as His98, Glu105 and His106.

Although both DtxR and Fur are iron-dependent repressor proteins, they regulate different groups of operators and do not substitute for one another in complementation tests [2,5]. DNA-protection experiments have confirmed that the specificities of DtxR and Fur for binding to operator sequences are different. It remains to be determined whether the general regulatory principles deduced from the studies on DtxR that we report here, will be applicable to the Fur protein.

Results

The crystal structure of DtxR was determined in the presence of six different cationic co-repressors, and in two different unit cells. The structures determined are very similar and appear to be quite insensitive to the type of co-repressor present. Significant differences were confined to one of the metal-binding regions.

Structure of the monomer

The polypeptide chain in the DtxR subunit could be traced for residues 4–144 and 168–191. It appears that each subunit contains two well-ordered domains and one less well-defined domain at the carboxyl terminus (Fig. 2). The amino-terminal domain (residues 1–73) contains three helices, two antiparallel β-strands, plus the first half

Fig. 4. The DtxR dimer. **(a)** Viewed along the two-fold axis, showing residues 4–144 and 168–191 in each subunit, with a dotted line connecting the carboxy-terminal end of domain 2 to domain 3. **(b)** The 'core' of the DtxR dimer, formed by the two DNA-binding and the two interface domains, viewed perpendicular to the two-fold axis. **(c)** Cavities in the core of the DtxR dimer, calculated by the program GRASP [22]. The purple and green cavities are located in the DNA-binding domains, the pink cavity is situated in the interface region of the dimer. (Figs 4a and 4b have been drawn with MOLSCRIPT [33] and RASTER3D [34,35].)

of the long helix α4 that runs from residue 66 to 88. The second domain (residues 74–144) is also mainly helical, containing helices α4, α5 and α6 (see the legend to Fig. 2 for a full description of the secondary-structure elements).

The topology of the first domain is similar to that of the DNA-binding domains in CAP [18], the globular domain of histone 5 (GH-5) [19] and the λ repressor [20]. Of these three proteins, CAP appears most relevant for comparison with DtxR. First, CAP is a dimer like DtxR, whereas GH-5 is monomeric. Second, the amino-terminal domain of DtxR shares a more extensive similarity with CAP than with λ (see Fig. 3).

Domains 1 and 2 of DtxR make numerous interactions with each other, mainly involving residues of helix α1 of domain 1 and helices α4 and α5 of domain 2. A hydrophilic cleft is found between the two domains, held by a salt bridge involving Glu20 from helix α2 of domain 1 and Arg80 from helix α4 of domain 2. Other important links between the two domains are made by two contacts between helices α1 and α5: the guanidinium group of Arg13 on helix α1 is at a distance of 3.5 Å from the carboxylate of Glu105 on helix α5, and the carboxylate of Glu9 of helix α1 is 2.7 Å from the $N^{\delta 1}$ of His106 on helix α5. The latter interaction might be crucial for the functioning of the repressor, as will be discussed later.

The less well-defined domain 3 has some helical content (Figs 2 and 4), but in view of its disorder we refrain from a detailed description of this domain. Its orientation with respect to the two other domains is different in the 'small cell' than in the 'large cell' (see the Materials and methods section). No function has yet been established for the residues of this domain, although replacement of Ala147 by valine resulted in inactivation of repressor activity [16]. It is of interest that the amino acid sequence of DtxR in the 1030(–) strain of *C. diphtheriae*, in comparison with the reference DtxR from strain C7(–), has six differences at the amino acid level in the carboxy-terminal region that do not affect repressor activity [10]. It is also of potential interest that the Fur protein only consists of 140 residues.

Structure of the DtxR dimer at 2.8 Å resolution

Although our crystals contained one subunit per asymmetric unit, a dimer with numerous intersubunit interactions is generated by a crystallographic two-fold axis. In the dimer virtually all of the intersubunit contacts involve domain 2, which is therefore called the 'interface domain'. The interface between the two monomers is quite extensive (Fig. 4), having a total buried accessible surface of 1687 $Å^2$, of which 1256 $Å^2$ is hydrophobic buried accessible surface.

The dimer interface can be described as consisting of three parts. The first area of contact comprises residues 104–108 of helix α5. Specifically, Trp104, Val107 and Met108 are involved in intersubunit hydrophobic interactions with their symmetry-related partners in the

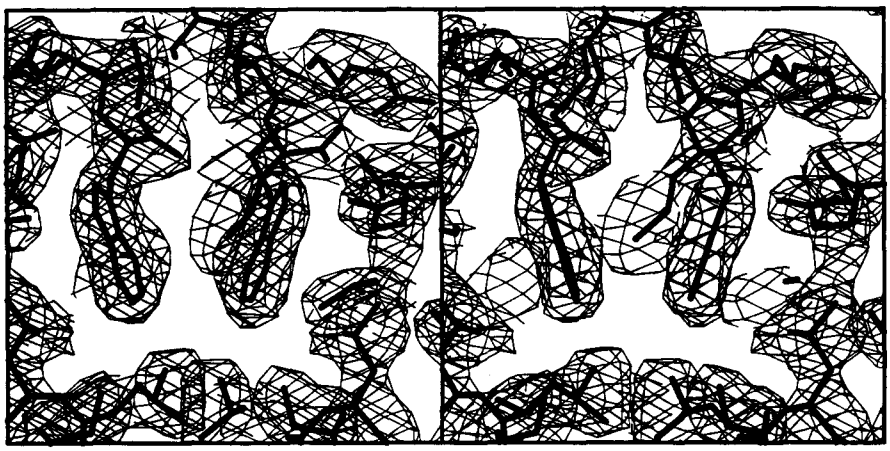

Fig. 5. Stereoview of the electron densities of Trp104 of each monomer at the dimer interface. The view is perpendicular to the crystallographic two-fold axis. The electron density shown is the final 2.8 Å $2F_o$–F_c map of the Fe–DtxR structure, contoured at 1.5σ.

other subunit. Interestingly, the indole rings of Trp104 and its counterpart, Trp104′, face each other across the dimer axis in such a manner that they are not in contact with each other (Fig. 5). Instead, they are separated by a small cavity, ~35 $Å^3$ in size. The second intersubunit contact area (which occurs twice) consists of residues 89–92 of the loop between helix α4 and helix α5, which interact with helix α5 of the other subunit. Residues Ile89 and Ile90 in particular contribute to the hydrophobic interactions of this interface. The third contact area is found across the two-fold axis between the amino-terminal residues 4–6 of each subunit. This region of the model has relatively high B-factors, however, and its contribution to the stability of the dimer might be quite limited.

Inspection of the packing in the DtxR dimer reveals the presence of one cavity per monomer in addition to the cavity in the interface region (Fig. 4c). The monomer cavity has a size of ~68 $Å^3$ and is lined entirely by the hydrophobic side chains of Tyr11, Ile15, Ile30, Val41, Val45, Val54, Met48, Leu62 and the hydrophobic part of Arg27. This cavity could provide sufficient space for two water molecules, but no evidence exists for such waters in the current electron-density maps. In view of the entirely hydrophobic nature of the wall of the cavity, it might not contain water molecules with any significant occupancy. This cavity could be relevant to conformational changes which this domain might undergo when forming the apo-repressor or when binding to DNA.

Metal-binding sites

Metal-binding site 1

In all of the structures of DtxR elucidated we observe one high peak at the same position in the difference Fouriers. In the F_{obs}–F_{calc} difference Fouriers of DtxR in the presence of $FeCl_2$, $MnCl_2$, $CoCl_2$ and $ZnCl_2$ (all in the large cell), and of $NiCl_2$ (in the small cell), this was the only major peak. In the case of $CdCl_2$, this was the highest difference Fourier feature. We refer to this site as 'metal-binding site 1'. The coordinating protein atoms are $N^{\epsilon 2}$ of His79, one or possibly both carboxylate oxygens of Glu83, and $N^{\delta 1}$ of His98. His79 and Glu83 are provided by successive turns of helix α4, and His98 is part of helix α5. A fourth ligand is provided by a well-defined solvent molecule or ion (labeled '303' in Fig. 6). This solvent ligand possibly interacts with the side chain of Asn130, although the ligand–side chain distance is 3.5 Å. In the refinement a water molecule at this position obtained a B-factor approximately equal to the average of the neighboring residues, and is therefore most likely a well-ordered water molecule or hydroxyl ion, but not a chloride ion. The coordination of the metal at binding site 1 is close to tetrahedral, with very reasonable metal-to-ligand distances (Figs 6 and 7). There is a kink in helix α4 between the two ligands His79 and Glu83,

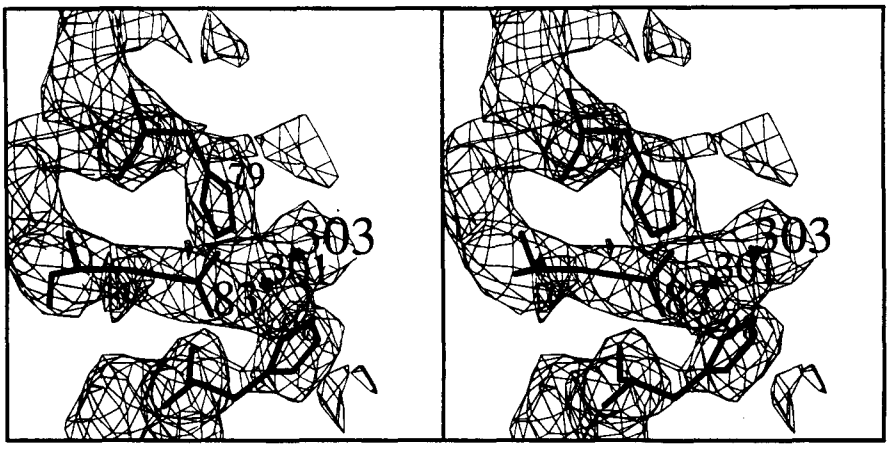

Fig. 6. Stereoview of the 2.8 Å $2F_o$–F_c electron-density map of Fe–DtxR near metal-binding site 1. The map is contoured at 1.5σ. His79 is on top, Glu83 to the left and His98 at the bottom. The * at the center, labeled 301, indicates the metal position and the * to its right, labeled 303, shows the position of the liganding solvent molecule.

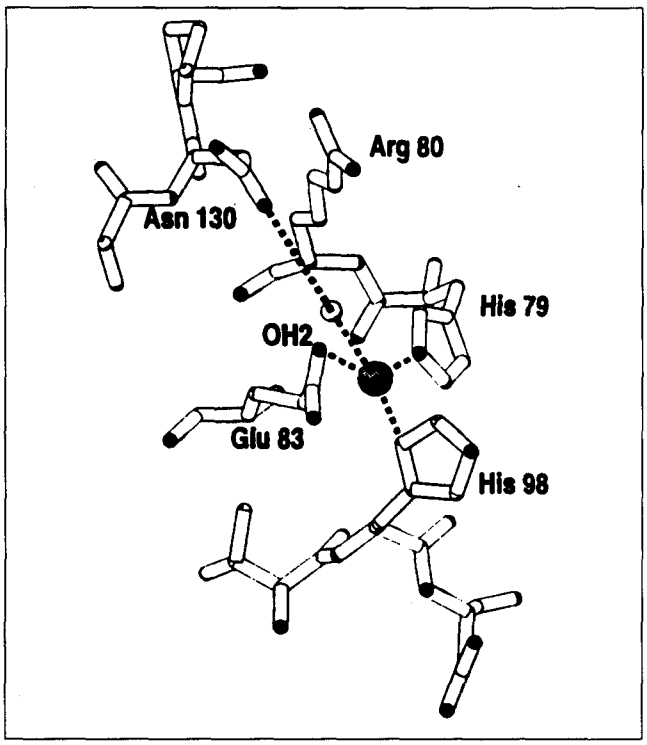

Fig. 7. Close-up view of the coordination at metal-binding site 1.

which could play a role in possible conformational changes induced by the binding of divalent metal ions.

The distance between the two metal sites 1 in the dimer is 29 Å. Although this precludes any possibility that the ligands of binding site 1 interact directly with the ligands of binding site 1 in the other subunit, a possible indirect route of communication is revealed by inspecting the location of metal-binding site 1 relative to the dimer interface region. One side of helix α5 provides the metal ligand His98, which makes contact with Cys102 on the same side of the helix, whereas on the other side of helix α5, Trp104 and Val107 make contact with their partners from a neighboring residue. Hence, metal binding at site 1 might influence the organization of this interface region and thereby affect the dimerization of DtxR. Conversely, dimerization could affect the organization of the metal-binding site 1. Whether or not this is physiologically relevant remains to be determined.

Metal-binding site 2

In the structure of DtxR in the presence of 2 mM $CdCl_2$ not one but two metal-binding positions are observed: metal-binding site 1, described above, and a second Cd-binding site located 9.6 Å away from metal-binding site 1, called 'metal-binding site 2'. In the Cd–DtxR structure, the second site is also approximately tetrahedrally coordinated, but is more distorted from ideal tetrahedral geometry than the first site. The four ligands are the carbonyl oxygen of Cys102, the $O^{\epsilon 1}$ atom of Glu105, the $N^{\epsilon 2}$ atom of His106, and a solvent molecule (Fig. 8a and Fig. 9). This latter solvent molecule is fully accessible to bulk solvent and does not interact with any other protein atom. This contrasts with the situation for metal-binding site 1, where the liganding solvent possibly interacts with the side chain of Asn130 (Fig. 7). Moreover, the first site contains two histidine ligands whereas the second site contains only one. These differences between the two metal-binding sites of DtxR suggest different metal affinities of each site.

The distance between the two binding sites 2 in the DtxR dimer is 17 Å. As for the first site, no direct interaction is possible between ligands of the sites 2. Ligands Cys102, Glu105 and His106 of metal-binding site 2 are, however, very close in sequence to Trp104, Val107, and Met108, which are at the core of the dimer interface (Figs 4 and 5). Metal-binding site 2, like binding site 1, could therefore affect dimerization as well as be affected by dimer formation.

Metal-binding site 2 is not occupied in any of the structures solved except for Cd–DtxR (Fig. 8). In the Cd–DtxR difference Fourier map, the peak at site 2 is significantly lower than at site 1 (see the Materials and methods section). Hence, the second site is not fully occupied even at a $CdCl_2$ concentration of ~2 mM. It should be pointed out, though, that our crystals were used for X-ray data collection several weeks to months after the initial set-up of the crystallization experiments, apparently leading to oxidation of the Cys102 sulfhydryl group. This was evident from several electron-density maps (Fig. 8). In the DtxR crystals obtained in the presence of $ZnCl_2$, $NiCl_2$, $MnCl_2$ (Fig. 8b) and $CoCl_2$ (plus 20 mM 2-mercaptoethanol), the S^{γ} appears to be a sulfenyl function (RSO^-). In the DtxR dimer obtained in the presence of 300 μM $FeCl_2$ plus 20 mM 2-mercaptoethanol over a period of several months, the difference Fourier shows two extra peaks of density near the S^{γ} of Cys102 which are compatible with a sulfinyl (RSO^{2-}) group (Fig. 8d). Also, in the crystals grown in the presence of $CdCl_2$ some evidence for the oxidation of Cys102 is observed. In view of the limited resolution of the Cd data and the possibility of series termination effects near heavy-atom positions in Fourier synthesis, it is therefore not possible to make definite statements about the oxidation state of Cys102 in the Cd–DtxR crystals on the basis of the crystallographic evidence available at present. Whether or not the lower metal occupancy reflects an affinity for Cd at site 2 that is intrinsically lower than that at site 1, or is a result of (partial) oxidation of Cys102, which prevents the S^{δ} atom from being engaged in metal coordination, needs further investigation.

It should be pointed out that the overall structures of DtxR in the presence of Fe and Cd are very similar. In the current structures of Fe–DtxR and Cd–DtxR, the C^{α} atoms of the first 140 residues superimpose within 0.6 Å, helices α3 superimpose within 0.3 Å, and the four coordinating atoms of metal-binding site 1 in the Cd- and Fe-containing repressors superimpose with a root mean square (rms) difference of 0.2 Å. Around the second Cd site, however, small shifts have occurred in one structure

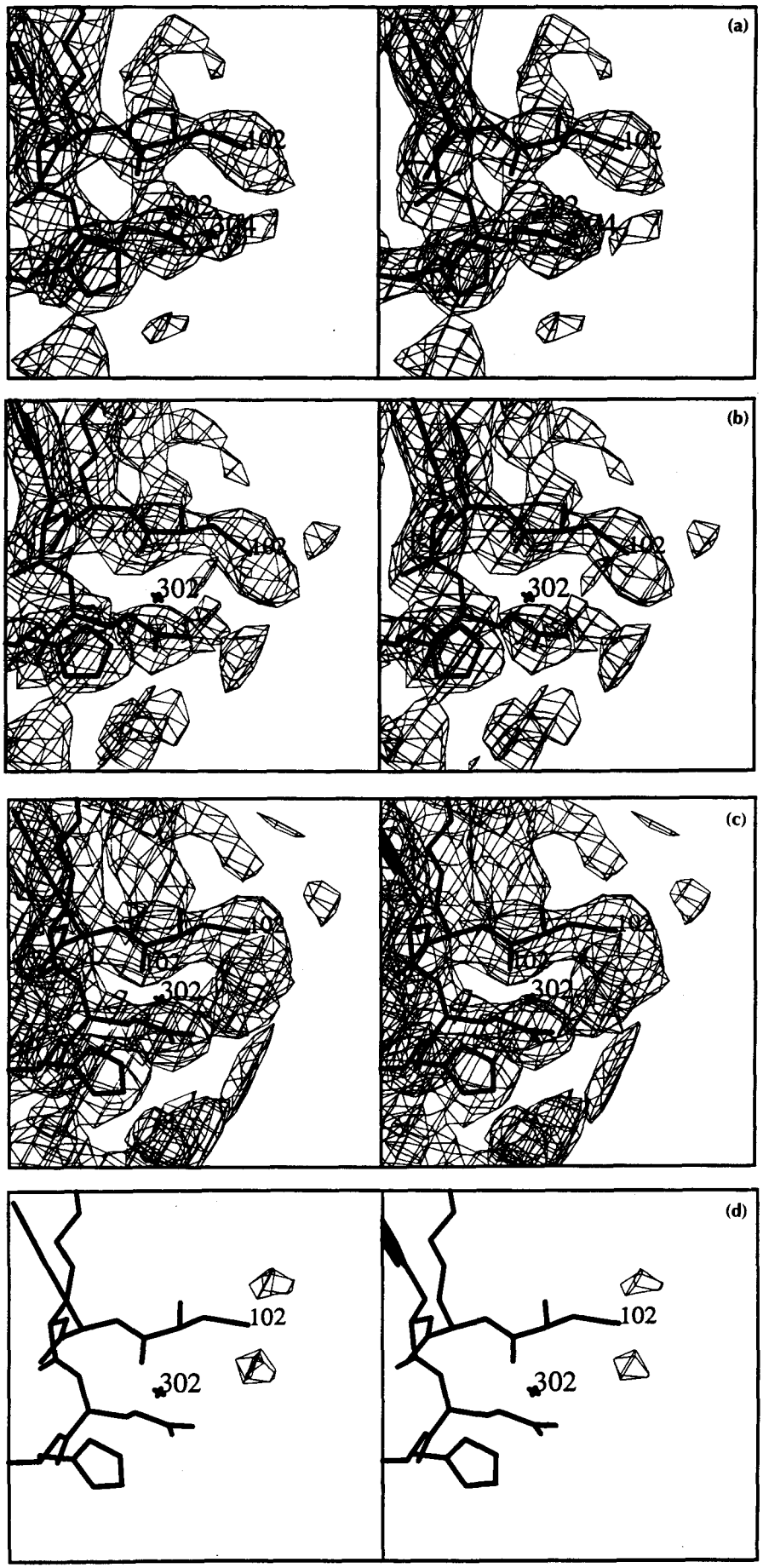

Fig. 8. Stereoviews of electron densities near metal-binding site 2. The ligand-providing residues are Cys102 at the top, Glu105 in the middle, and His106 at the bottom. The * in the center, labeled 302, indicates the metal position. **(a)** The second Cd site in the 2.8 Å $2F_o$–F_c map of Cd–DtxR contoured at 1.2σ. The water ligand is indicated by an *, labeled 304, to the right of the metal. **(b)** The Mn–DtxR 2.8 Å $2F_o$–F_c map at 1.2σ. The metal site is clearly unoccupied, and the Cys102 sulfur is probably oxidized to the RSO^- state. **(c)** The Fe–DtxR 2.8 Å $2F_o$–F_c map at 1.2σ. The metal site is also empty in this case. **(d)** The 2.8 Å F_o–F_c difference map of Fe–DtxR contoured at 3σ, clearly showing evidence for RSO_2 formation of Cys102.

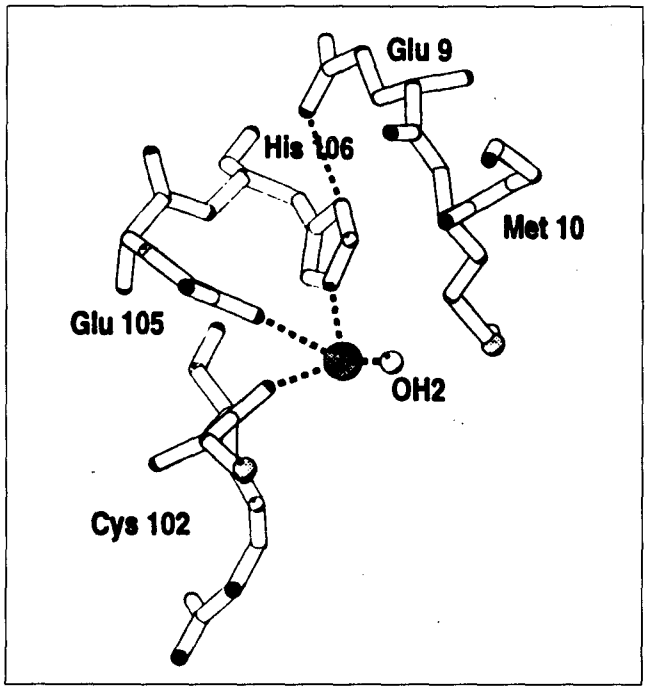

Fig. 9. Close-up view of the coordination at metal-binding site 2. The metal ligands Cys102, Glu105 and His106 are provided by helix α5 of the second domain. Residue Glu9 of helix α1 of the DNA-binding domain interacts with the metal coordinating His106.

relative to the other. The largest shift was observed for the S^{δ} atom of Met10, which is shifted by ~3 Å. The second largest shift of 1.1 Å is made by the $O^{\epsilon 2}$ of Glu9, which in the Cd structure interacts with the $N^{\epsilon 2}$ of His106. The latter atom is shifted by 1.0 Å. The carbonyl oxygen of Cys102 has only shifted by 0.2 Å. These numbers ought to be considered with some caution, however, because at a resolution of 2.8 Å certain changes might be masked by imperfections of the models, even though the R-factor was reduced to 21%. Nevertheless, DtxR seems able to accommodate a Cd ion at its second binding site with only a few local structural changes compared with the empty site in the Fe–DtxR complex.

The position of Cys102

As the only cysteine in the protein, Cys102 has provoked various interesting studies because cysteines have often been observed to be metal ligands [12]. In the structure of DtxR, however, Cys102 is not a direct ligand of metal-binding site 1. The S^{γ} of Cys102 is, nonetheless, in contact with the imidazole ring of His98, one of the direct metal ligands at the metal-binding site. Actually, the S^{γ} is only 3.7 Å from the $N^{\epsilon 2}$ of His98, implying that most of the side-chain mutations of Cys102 are likely to affect the precise positioning of His98, which could then distort the tetrahedral conformation of metal-binding site 1 and decrease the cation affinity of this site dramatically.

Interestingly, Cys102 is indeed involved in the direct coordination of the Cd ion at metal site 2 but, in the present structure, with a (partially) oxidized cysteine side chain, via its main-chain carbonyl oxygen, and not via its S^{γ} atom. It is noteworthy that the distance between the S^{γ} atom of Cys102 and the Cd atom at metal-binding site 2 is only 4.5 Å. Whether or not the S^{γ} of Cys102 might be a metal ligand in fully reduced DtxR still needs to be established.

Discussion

The disulfide-bridged dimer

The position of the two Cys102 residues in the dimer is most intriguing in view of the observation that DtxR, upon exposure to air, gradually forms inactive dimers that can readily be converted into active repressor by treatment with reducing agents such as 2-mercaptoethanol [9]. In the dimer, as revealed by our crystal structures, the distance between the two S^{γ} atoms is 23 Å. This makes the formation of the oxidized dimer quite puzzling. Cys102 lies in a gentle depression at the surface of the protein, where its side chain is quite accessible to solvent. Simple rigid-body docking experiments show that the disulfide-bridged dimer cannot be formed with the conformation of the monomers as observed in our structure. The disulfide-linked dimer could, however, be formed after a considerable conformational change, such as a complete rearrangement of helix α5, exposing Cys102, so that it could form a disulfide link with a Cys102 of another similarly rearranged monomer. Another conformational change could possibly be an opening of the angle between the DNA-binding and interface domains, such that the Cys102 S^{γ} is in a less deep depression at the surface, and can covalently be coupled to another subunit that has undergone a similar hinge-bending motion. Further experiments are obviously required to elucidate the structure of the covalently bridged DtxR dimer.

Mode of DNA binding

When viewed perpendicular to the two-fold axis (Fig. 4b) the 'core' of the DtxR dimer, formed by the first two domains of each subunit, resembles the shape of a butterfly. The interface domains form the 'body' and the lower halves of the 'wings', while the two amino-terminal domains point upwards and form the upper halves of the wings. No mutual contacts are formed between the amino-terminal domains except between the amino-terminal residues 4–6 of both monomers. Helices α3 of the first domain are located at the 'top' of the DtxR dimer. The position of helices α3 is intriguing because they contain Arg47, a residue for which substitution by histidine diminishes DNA binding [14]. Additional residues in helices α3 for which amino acid substitutions cause loss of repressor activity include Pro39, Thr40, Thr44 and Ala46 [16]. The distance between the two Arg47 residues in the dimer is ~30 Å — a distance observed frequently between DNA-binding helices [21]. Also, the axes of the α3 helices in the two subunits run nearly parallel to each other, with an angle of ~20° between them. These observations suggest that helix α3 is a major factor in DNA binding.

Three possible models for DtxR–DNA complexes have to be considered. In the first, the two putative DNA-binding helices α3 bind more or less in the major groove of the *tox* and *irp* operators, with the DtxR dimer axis coinciding with the pseudo dimer axis of the partially palindromic DNA sequence to be recognized. In the second model, the operator lies in the groove formed by the wings of the butterfly, with the DNA helix axis running perpendicular to the DtxR two-fold axis and roughly parallel to the axes of helices α3. In this DNA-binding mode the orientation of the DNA helix differs by 90° from that in the first model. Finally, the DNA binding mode could be significantly different from either of the first two models, because of, for example, a major conformational change in the repressor or a major deviation from the canonical B-DNA conformation in the double-stranded nucleic acid bound form.

Approximate electrostatic potential calculations made with the program GRASP [22] provide information that allows us to discriminate between the first two of these possibilities. As shown in Fig. 10, the electrostatic potential in the cleft between the two wings of the butterfly is negative, making it an unlikely place for contacts with the negatively charged deoxyribose-phosphate backbone of DNA. Regions of positive potential are observed at the amino-terminal ends of helices α3, making interactions of these regions with DNA a distinct possibility, in agreement with the first model mentioned above.

A comparative analysis of other dimeric DNA-binding proteins has provided useful additional information. A search of the Brookhaven Protein Data Bank for structures similar to DtxR using the program DEJAVU (kindly provided by Drs G Kleywegt and TA Jones) picked up CAP [23] as the protein having the greatest similarity to DtxR. The structural similarity is limited to the carboxy-terminal DNA-binding domain of CAP, which corresponds in topology with the amino-terminal DNA-binding domain of DtxR. The similarity in topology includes all three α-helices of the DNA-binding domains in the two proteins as well as both β-strands (see also Fig. 3). Wang *et al.* [16] have aligned the sequences of CAP and DtxR, and their alignment of the α2-turn-α3 motifs is close to, but not identical with, that obtained by our structural comparison. Structural similarity with the DNA-binding domains of GH-5 and the λ repressor (Fig. 3) is also significant. The helix-turn-helix motifs in these proteins superimpose quite well, with DtxR deviating from CAP, GH-5 and λ repressor by 0.68 Å, 1.00 Å and 0.65 Å for 20, 20 and 15 C^{α} atoms respectively. The amino acid sequence alignment resulting from these structural comparisons is given in Fig. 11, and indicates that these helix-turn-helix motifs share only a very limited sequence similarity.

The structural comparison between CAP and DtxR was extended to include the relative position of the DNA-binding motifs in the dimers. It appears that the C^{α} positions of the two α3 helices of the DtxR dimer

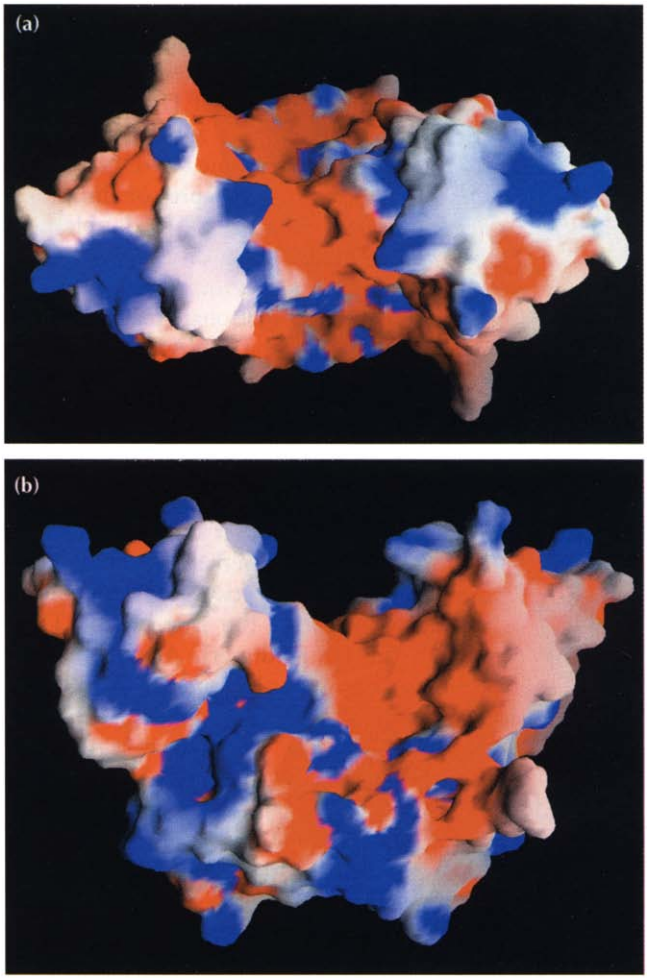

Fig. 10. Molecular surface of the DtxR dimer, color coded according to electrostatic potential as calculated by the program GRASP [22]. Four divalent cations of the DtxR dimer are included in the calculation. Dark blue corresponds to a potential >+3.0 kT/e^{-1}, red to a potential <–3.0 kT/e^{-1}. **(a)** View along the two-fold axis. **(b)** View perpendicular to the two-fold axis. Notice the positive potential around the recognition helices α3 that should allow for binding of the phosphate backbone of the DNA. The large areas with negative potential might be important for preventing unproductive DNA binding.

can be superimposed within 2.5 Å onto the two equivalent helices of the CAP dimer in the CAP–DNA complex [18]. Apparently, not only are the mutual arrangements of the secondary-structure elements within the DNA-binding domains of DtxR and CAP analogous, but the mutual positions and orientations of these domains in the dimers are also quite similar. This provides support for a model of the DtxR–DNA complex which is analogous to that of the CAP–DNA complex: the dimer axis of holo-repressor coincides with the pseudo two-fold axis of the bound DNA. Further support for this binding mode, model 1 described above, comes from the observations that the region of the *tox* and *irp* operators to which DtxR binds contains a palindromic sequence [13].

Superposition of the CAP–DNA complex onto DtxR yields a model of the DtxR–DNA complex in which the

α3 helices of the DtxR fit reasonably well into the major groove of DNA, but the large bending angle of the CAP–DNA causes several clashes between the nucleic acid and the DNA-binding domain of DtxR (data not shown). Another way of arriving at a model of DNA bound to DtxR is to start from canonical B-DNA and fit this onto the DtxR dimer with the repressor dimer axis coinciding with the dimer axis of the DNA double helix (Fig. 12). Because the middle region of the CAP–DNA complex is quite straight in this region, the two models are very similar. Ignoring the rotational freedom of the DNA about the two-fold axis, the DNA can still adopt two possible orientations with respect to the dimer, but only the DNA orientation shown in Fig. 12 permits the α3 helices to fit well into the major grooves. Such a model of straight DNA in complex with DtxR avoids the numerous collisions in the model based on the CAP–DNA bent helix, but has other shortcomings. For example, this model does not predict significant protein–DNA interactions near the two-fold axis of the complex (in particular, not on the side of the DNA pointing away from the DtxR dimer). Also, few if any protein–DNA interactions occur beyond the 7 bp region flanking the dyad axis of the complex (Fig. 12). This model of straight DNA with DtxR cannot therefore explain the results obtained by hydroxyl radical DNA protection experiments (see Fig. 1) [13,14].

Further analysis suggests that protection of DNA against hydroxyl radicals in the center of the bound double-stranded DNA might be caused by a rearrangement of the amino-terminal residues of DtxR. These amino termini cross the crevice between the two DNA-binding domains in our structure, and residues 1–3 appear to be flexible. They might well undergo a major rearrangement and interact with the nucleic acid once repressor–operator complexes are formed. Such interactions are analogous to the central region of DNA bound to λ repressor [19], where the amino termini of the repressor protect the DNA backbone on the side of the DNA pointing away from the protein. The amino termini might, therefore, have a similar function in the λ and diphtheria toxin repressors.

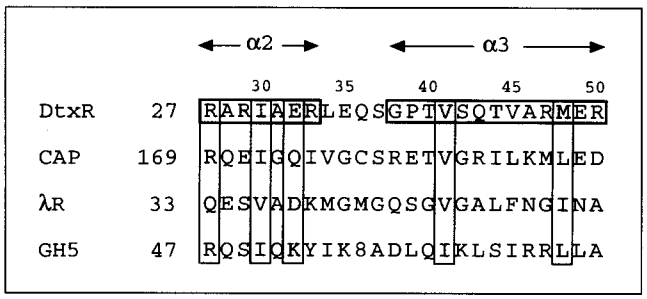

Fig. 11. Alignment of helix-turn-helix sequences in DtxR, CAP, λ repressor and GH5. Positions of conserved amino acids boxed horizontally. Helices α2 and α3 as occurring in DtxR are boxed vertically. The equivalent helices in the other proteins can deviate slightly from that in DtxR. The symbol 8 in the sequence of GH5, signifies an eight-residue insertion.

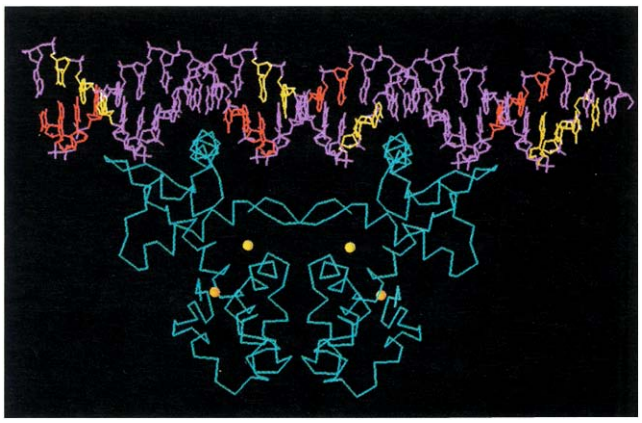

Fig. 12. Mapping the results of footprinting experiments with the *tox* operator [13] onto a model of canonical B-DNA (magenta) in complex with the experimental DtxR core structure (blue). Parts of the DNA sequence protected from hydroxyl radical cleavage by DtxR are depicted in red (one strand) and yellow (the other strand). The lower pair of yellow spheres in each subunit represents metal-binding sites 1, the upper yellow spheres metal-binding sites 2. The strictly conserved ends of the palindromic sequence (AGG[N_9]CCT), in the centers of the major grooves, are in contact with the two α3 recognition helices of DtxR. Note that residues 1–3 are not shown because their density is too weak in electron-density maps.

The model of DtxR in complex with straight DNA also fails to explain why bases at the ends of the operator, i.e. beyond the central 15 bp, are protected (Fig. 12). Because the strongly bent DNA as in the CAP–DNA complex leads to unacceptable clashes, it is likely that in the DtxR–DNA complex the DNA is bent to a somewhat smaller degree than in CAP. Examples of less strongly bent DNA recognized by proteins are the λ [20] and the Cro repressor [24] DNA complexes. Superpositions of the λ and Cro dimers onto the DtxR dimer showed, however, significant deviations in the orientations of the helix-turn-helix motifs in the two subunits of DtxR, λ and Cro. This is not surprising given the significant differences in arrangement of the helices in the DNA-binding domains of DtxR and λ (see Fig. 3). Clearly, obtaining an accurate model for DNA binding by DtxR will almost certainly have to await the structure determination of a DtxR–DNA complex.

The role of the third domain of DtxR is unclear. It is definitely not involved in any dimer contacts, and it is also far removed from DNA in the most likely DtxR–DNA complex. A dramatic conformational change of the third domain might enable it to participate in binding to its cognate operators, or it could have as yet unknown functions.

Explanation of mutant phenotypes and action of co-repressor

The residue that has been the subject of the most intensive mutational studies is Cys102. It is not a ligand of metal-binding site 1, and its side chain also does not interact with the metal at binding site 2, hence the loss of

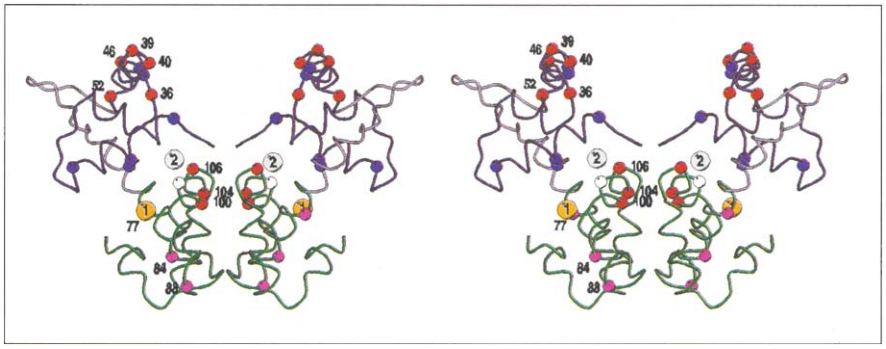

Fig. 13. Stereoview of the core of the DtxR dimer showing amino acid substitutions that impair the repressor activity [16]. A C^{α} trace of the first two domains is shown, with residues 1–3 of each subunit omitted because these are not sufficiently well defined in the electron-density map. The helix-turn-helix motif is coloured dark blue, the rest of the domain 1 gray and domain 2 green. The effects of the substitutions, assessed at the phenotypic level, are color-coded according to severity of loss of DtxR activity: mild (dark blue), serious (magenta) and severe (red). The sequence numbers of residues that, when substituted, affect repressor activity seriously or severely are indicated. Residue Cys102 is shown in white. The yellow spheres represent metal-binding site 1 in each subunit, the gray spheres indicate metal-binding sites 2.

repressor activity as a result of all but one (Cys102→Asp) substitution made at this position [12] is likely to be attributable to indirect effects of the newly introduced side chain upon metal binding. A special case is the mutation Cys102→Pro. Because Cys102 resides in a helical region of the polypeptide chain, a proline at position 102 will change the course of the backbone and thereby could affect both metal-binding sites. For the other substitutions it is important that the S^{γ} of Cys102, as mentioned before, is only 4.5 Å away from metal-binding site 2 and is also in contact with His98, a ligand of metal binding site 1. Hence substitutions of Cys102 by other residues might affect both metal sites and hence metal affinity, as well as DNA recognition. It is perhaps more difficult to explain why the Cys102→Asp mutant has some residual repressor activity [12] than why other mutants have no activity. It might be that an O^{δ} atom of Asp102 in the Cys102→Asp mutant is coordinating the metal at binding site 2 without significant conformational changes in the holo-repressor.

One possible way in which metal co-repressors could be utilized for repressor regulation is by situating them at the protein–DNA interface, thus involving the metal directly in repressor–DNA binding. Apparently, this is not the case for metal regulation of operator affinity in DtxR, as the positions of both metals are far removed from the proposed DNA positions (Fig. 12). Therefore, an indirect mode of action of the co-repressor, involving a conformational change of DtxR, is expected.

When amino acid residues for which substitution variants have been characterized are projected onto the backbone of the DtxR dimer and colored according to the degree of inactivation of repressor activity caused by these substitutions, two clusters of important residues are immediately obvious (Fig. 13). One cluster occurs at the 'top' of the molecule and consists of residues in the DNA-binding α2-turn-α3 motif. The other cluster consists of residues 100, 102, 104 and 106, which are all close to metal-binding site 2. This site is located between the first and second domains of DtxR. As mentioned before, the site 2 ligand His106 interacts with Glu9 (Fig. 9) which is located at the very beginning of helix α1. This helix might not interact directly with bound DNA, but it is in intimate contact with both helices 2 and 3, the helix-turn-helix DNA-binding motif.

These observations suggest that metal binding at site 2 might be crucial for orienting the DNA-binding domain correctly with respect to the interface domain so that a proper DtxR–DNA complex can be formed. Rotation of DNA-binding domains has been reported for the Trp repressor [25], where the co-repressor Trp orients the DNA-reading heads for proper interaction with the target DNA. Another example is CAP, where a rotation of the DNA-binding domain with respect to the carboxy-terminal domain of not less than 28° has been reported [18,23]. This is quite relevant for our study, because the CAP and DtxR DNA-binding domains are very similar (Fig. 3). The structure of DtxR, with the cleft between the DNA-binding and interface domains, seems to be well suited for a similar type of rotation to occur when apo-DtxR binds metal or when the holo-repressor binds its cognate DNA.

We propose that in the DtxR dimer the co-repressor is the key to orienting the DNA-binding domains with respect to the interface domains, and hence with respect to each other, so that the DNA-binding reading heads are optimally positioned for DNA binding. In view of the cluster of mutations near metal-binding site 2, and the strategic location of that site in the contact region of the DNA-binding and interface domains, it is tempting to propose that metal-binding site 2 is more essential than binding site 1 for modulating the repressor activity of DtxR. Clearly, further structural investigations are needed to determine the difference between apo- and holo-repressor, and the occupancy and function of both metal-binding sites in fully reduced holo-repressor.

The DtxR structure reported in this paper answers many questions regarding the architecture of this medically relevant and prototypic prokaryotic global regulatory protein. It provides a framework for understanding the function of DtxR, the first iron-dependent repressor protein for which a three-dimensional structure has been solved.

Biological implications

The low iron concentration of ~10^{-18} M in the human host is a first line of defence against infectious diseases, but serves also as a signal for expression of virulence factors and iron-uptake systems by most pathogenic bacteria. Two well-characterized repressor families are involved in the iron-dependent expression of virulence factors: the Fur protein in *Escherichia coli, Vibrio cholerae, Yersinia pestis, Pseudomonas aeruginosa* and related Gram-negative bacteria, and the diphtheria toxin repressor (DtxR) in *Corynebacterium diphtheriae*. DtxR is a dimeric protein which can bind not only to Fe(II) but also to Mn(II), Ni(II), Cd(II), Zn(II) and Co(II). The resultant holo-repressor binds to specific operators and prevents transcription from their associated promoters. At low cation concentrations, the metal ions are no longer bound to DtxR, and the apo-repressor loses its affinity for the operators. In *C. diphtheriae* such derepression triggers the synthesis of various products, including diphtheria toxin, an ADP-ribosylating toxin which irreversibly modifies elongation factor 2, resulting in cell death and contributing to the pathogenesis of diphtheria. The present study addresses the structural basis for the iron-dependent repression by DtxR of virulence factor gene expression in *C. diphtheriae*.

The three-dimensional structure of the DtxR dimer reveals that each subunit consists of three domains, with a core formed by the first two domains, which have distinctly different functions. The amino-terminal domain is responsible for DNA binding, the second domain for dimerization and metal binding. This architecture suggests how the co-repressor may work. The divalent cations bind to a metal-binding site at or near to the interface of two domains in each subunit, thereby probably controlling the orientation of the amino-terminal DNA-binding domain with respect to the interface domain. This orientation determines the distance between the DNA-binding regions in the two subunits and thereby the affinity for DNA. The DNA-binding domain has the topology of the helix-turn-helix motif observed in several other dimeric DNA-binding proteins. Structural comparison of DtxR with these proteins, in particular catabolite gene activator protein (CAP), in conjunction with studies with mutant forms of DtxR, shows that helix α3 is a major DNA-recognition element. Molecular modeling suggests that DNA is probably bent when bound to DtxR but less so than when bound to CAP.

Major principles of iron-regulated expression of virulence factors in a variety of important human pathogens are explained by our structural investigations. They form the basis for further studies, several of which will be of potential therapeutic interest.

Materials and methods

Purification and crystallization

DtxR was expressed and purified as described previously [14]. Vapor-diffusion hanging-drop crystallization trials were initialized employing a series of factorial conditions developed in this laboratory (S Sarfaty, X Qiu, S Mande, L Stewart and WGJ Hol, unpublished data). Small crystals, grown over a period of 3 months, were obtained with a 2.0 M $(NH_4)_2SO_4$ well solution in 0.1 M Tris buffer, pH 8.0, and a drop containing 3 mg ml^{-1} protein, 0.5 mM $CoCl_2$, 50 mM Tris, pH 8.0, 1.0 M $(NH_4)_2SO_4$ and 20 mM 2-mercaptoethanol. The quality of the crystals was improved by carefully adjusting precipitant concentrations and pH, which yielded large single crystals, with dimensions of 0.9 mm×0.4 mm×0.3 mm, of DtxR in the presence of cobalt ions in less than 1 week. Under similar conditions, crystals of DtxR in the presence of $FeCl_2$, $MnCl_2$, $NiCl_2$, $ZnCl_2$, $CdCl_2$ and 1 mM EDTA were also obtained, but some of these crystals grew only after several weeks. The presence of metal ions in the crystals could sometimes be judged by the distinct color of the crystals.

Data collection and heavy-atom derivative search

X-ray diffraction data were collected using a Siemens multiwire area detector, an RAXIS-II imaging plate (both equipped with a Rigaku RU-200 rotating anode generator), as well as a Mar Research imaging plate at beam line 7-1 of the Stanford Synchrotron Radiation Laboratory (SSRL). Intensity data were processed with XENGEN [26], the RAXIS software and MOSFLM [27]. The crystals diffracted X-rays to better than 2.8 Å resolution in most cases. Statistics of the data sets that are used in various calculations are listed in Tables 1 and 2.

Data were collected from two different kinds of $P3_121$ crystals, one with a 'large' unit cell (a=b=64 Å, c=109 Å) and another with a 'small' cell (a=b=63.5 Å, c=105.5 Å). The two crystal forms are not isomorphous, as indicated by an R-factor of 42% between the two data sets. These crystals contain only one monomer per asymmetric unit. The calculated solvent content is ~50% with V_m=2.6 $Å^3$ Da^{-1}. In searching for heavy-atom derivatives, over 50 compounds were explored and ~100 data sets were collected. Native ('NAT' in Table 1; grown from a solution containing 1 mM EDTA) and heavy-atom derivative crystals 'Cd' (2 mM $CdCl_2$), 'Hg1' (2 mM $HgCl_2$) and 'Hg2' (10 mM $HgCl_2$) were obtained through co-crystallization, whereas the 'CM1', 'CM2', 'EMC', 'PS1', 'PS2' and 'HgI' crystals were prepared by soaking the crystals into, respectively, saturated chloromercurinitrophenol, saturated ethylmercurichloride, 10 mM *p*-chloromercuribenzenesulphonate, and 0.5 mM K_2HgI_4/KI for 2–3 days. In all of the soaking trials, $(NH_4)_2SO_4$ was replaced by 1.5 M Li_2SO_4 as the stock solution, to decrease the possibility of free NH_3 interfering with the binding of heavy metal compounds to DtxR.

Structure determination and refinement of native crystal

The structure of the DtxR was initially solved by the multiple isomorphous replacement plus anomalous scattering (MIRAS) method, treating the data from crystals grown in the presence of 1 mM EDTA as the native data set. Most of the calculations were done using the CCP4 program suite [28]. Nine derivatives were identified, first from difference Patterson maps and

Table 1. Multiple isomorphous replacement data and phasing statistics.

	NAT	Cd	Hg1	Hg2	CM1[a]	CM2	EMC	PS1	PS2	HgI
Max. resolution (Å)	2.8	2.8	2.8	3.0	3.5	2.8	3.2	2.8	2.8	3.1
Detector	Raxis	Raxis	Raxis	Mar	Siemens	Raxs	Siemens	Raxis	Raxis	Raxis
R_{merge}[b]	0.052	0.058	0.055	0.098	0.092	0.080	0.112	0.113	0.098	0.066
Completeness (%)[c]	88	85	70	92	88	78	90	60	77	68
R_{iso}[d]	–	0.11	0.13	0.34	0.21	0.22	0.19	0.14	0.15	0.13
No. of sites	–	3	10	10	3	3	4	5	5	5
R_{Cullis}[e]	–	0.81	0.84	0.72	0.71	0.69	0.78	0.83	0.82	0.86
Phasing power[f]	–	1.3	0.9	1.6	1.7	1.6	1.2	1.0	0.8	0.9

[a]Anomalous diffraction data are included. [b]$R_{merge} = \Sigma|I - \langle I \rangle|/\Sigma\langle I \rangle$, where I is the observed intensity and $\langle I \rangle$ is the average intensity of multiple observations. [c]Percentage of theoretically possible reflections that is available and used in calculations. Reflections with $F < 2\sigma(F)$ are rejected. [d]$R_{iso} = \Sigma|FPH - FP|/\Sigma|FP|$, where FP and FPH are the observed native and derivative structure-factor amplitudes. [e]$R_{Cullis} = \Sigma|FH_o - FH_c|/\Sigma|FH_o|$, where FH_o and FH_c are the observed and calculated heavy atom structure-factor amplitudes for centric reflections. [f]Phasing power is the rms isomorphous difference divided by the rms residual lack of closure. (See Materials and methods for description of conditions for producing heavy-atom derivtives.)

Table 2. DtxR structure refinement statistics.

	Fe	Cd	Mn	Zn	Co	Ni
Max. resolution (Å)	2.8	2.8	2.8	2.8	2.8	2.8
Detector	Raxis	Raxis	Raxis	Raxis	Raxis	Raxis
Unit cell a/c (Å)	64.56/108.58	64.05/108.91	63.83/109.46	63.96/109.05	63.90/109.34	63.41/105.30
R_{merge}	0.082	0.058	0.101	0.044	0.035	0.081
Completeness (%)	71	85	75	84	92	83
Final R (6.0–2.8 Å)	0.211	0.229	0.227	0.243	0.262	0.271
Rms bond length (Å)	0.016	0.017	0.018	0.016	0.018	0.019
Rms bond angle (°)	2.3	2.2	2.4	2.3	2.2	2.3
$(F_o - F_c)$ peak at site 1	11σ	9σ	7σ	7σ	9σ	7σ
$(F_o - F_c)$ peak at site 2	–	5σ	–	–	–	–

later from difference Fourier maps. The program MLPHARE [29] was used for heavy-atom parameter refinement and phase calculation. The final figure of merit was 0.60 for the reflections from 50.0 Å to 2.8 Å. The resulting electron-density map clearly showed the six major helices, including most of the side chains. This allowed the determination of the direction of the polypeptide chain. Density modification, including solvent flattening, histogram matching and application of Sayre's equation, was carried out using programs in the CCP4 suite. The improvements were quite remarkable in regions where the MIRAS density was reasonably good. The sequences of the helices could then be readily assigned, so providing information about the connections between the helices.

Model building was carried out with the molecular graphics program O [30] and facilitated by its BONES option. The initial model from the density-modified map consisted of 121 residues, of which 80% had side chains. The starting R-factor for the reflections between 10 Å and 2.8 Å resolution was 43.2%. Forty cycles of positional refinement, as well as 20 cycles of overall and restrained individual temperature-factor refinement by X-PLOR version 3.1 [31], brought the R-factor down to 35.5%. Calculated phases from this partial model were then combined with the original MIRAS phases, and an F_o electron-density map was calculated using the combined phases and the figure of merit as weighting factor. Subsequent model building, additional cycles of refinement, phase combination and $(2F_o–F_c)$ synthesis with combined and, later, calculated phases were carried out. Simulated annealing using the X-PLOR slow-cooling protocols was also performed in the later cycles of refinement.

The program PROCHECK [32] was used to check the stereochemical and geometric outliers. The current model consists of the well defined residues 4–59, 61–136, and the less well defined residues 60, 137–144 and 168–191. Without adding waters, the current R-factor is 22.9% using all the native data between 6.0 Å and 2.8 Å. The rms deviations from ideality of bond distances and angles are 0.017 Å and 2.3° respectively. Further refinement, including the addition of well defined solvent molecules, will be carried out in the near future.

Metal-binding site 1 is correlated with a $(F_o–F_c)$ difference peak of 7.5σ, indicating the presence of a partially occupied metal in the native crystal, in spite of the presence of 1 mM EDTA in the crystallization mother liquor. Therefore, an apo-DtxR structure is still lacking. Because the protein was purified using a nickel-containing affinity column [14], the density at metal-binding site 1 in the 1 mM EDTA crystal could be attributable to the presence of nickel ions. Soaking of crystals into solutions containing 5 mM EDTA cracked the native 1 mM EDTA crystals, as well as Co–DtxR and Zn–DtxR crystals. This crystal cracking suggests that apo- and holo-DtxR could have quite different conformations.

Structure determination of other DtxR crystals

The crystals of DtxR grown in the presence of $FeCl_2$, $CdCl_2$, $MnCl_2$, $ZnCl_2$ and $CoCl_2$ are isomorphous with the native

crystals. The structures of these metal–DtxR complexes could therefore be solved by using the native structure as a model and performing positional refinement, simulated annealing and individual temperature-factor refinement. The current stage of refinement of each of these structure determinations is given in Table 2. Detailed refitting of each of the structures will be carried out in the near future.

The Ni–DtxR crystals have the 'small' unit cell. Therefore, molecular-replacement procedures were applied to solve this structure. Residues 4–136 of the native DtxR model obtained in the 'large' cell were used as the search model. The rotation and translation function solutions, obtained with X-PLOR [31], had peak heights of 10σ and 12σ respectively. Rigid-body refinement, positional refinement, simulated annealing and individual temperature-factor refinement brought the R-factor down to 27% (Table 2) without any manual refitting of the model. Superposition of the native DtxR structure and the Ni–DtxR model revealed that the third domain must be oriented differently in the small cell as the 'large cell orientation' of this domain causes an unacceptable overlap with symmetry-related molecules in the small cell. This indicates that the polypeptide chain linking the second and third domains is highly flexible. Despite the obvious differences in unit cells and third-domain orientations, the structures of the first two domains are nearly identical in native and Ni–DtxR, especially near the metal-binding sites. Detailed comparisons of all the structures will be reported elsewhere. The observed peak heights of the (F_o–F_c) difference electron density at both metal sites in the various metal–DtxR complexes are listed in Table 2.

Atomic coordinates of the DtxR have been deposited in the Brookhaven Protein Data Bank with access code 1DTR.

Acknowledgements: We thank Stewart Turley for assistance with data collection, Ethan Merritt for assistance with computations and preparation of figures, Steve Sarfaty for his invaluable advice on crystallization, and Edda Twiddy for advice on purification of DtxR. We are indebted to the Murdock Charitable Trust for a major equipment grant to the Biomolecular Structure Program. RKH acknowledges support from the National Institute of Health (grant AI14107). The opinion and assertions expressed herein are those of the authors and not necessarily the views of the Uniformed Services University of the Health Sciences or the Department of Defense. We would also like to extend our acknowledgements to the support of SSRL for synchrotron data collection.

References

1. Litwin, C.M. & Calderwood, S.B. (1993). Role of iron in regulation of virulence genes. *Clin. Microbiol. Rev.* **6**, 137–149.
2. Tai, S.P. & Holmes, R.K. (1988). Iron regulation of the cloned diphtheria toxin promoter in *Escherichia coli*. *Infect. Immun.* **56**, 2430–2436.
3. Boyd, J. & Murphy, J.R. (1988). Analysis of the diphtheria *tox* promoter by site-directed mutagenesis. *J. Bacteriol.* **170**, 5949–5952.
4. Tai, S.P., Krafft, A.E., Nootheti, P. & Holmes, R.K. (1990). Coordinate regulation of siderophore and diphtheria toxin production by iron in *Corynebacterium diphtheriae*. *Microb. Pathog.* **9**, 267–273.
5. Boyd, J., Ova, M.A. & Murphy, J.R. (1990). Molecular cloning and DNA sequence analysis of a diphtheria toxin iron-dependent regulatory element (DtxR) from *Corynebacterium diphtheriae*. *Proc. Natl. Acad. Sci. USA* **87**, 5968–5972.
6. Schmitt, M.P. & Holmes, R.K. (1991). Characterization of a defective diphtheria toxin repressor (*dtxR*) allele and analysis of *dtxR* transcription in wild type and mutant strains of *Corynebacterium diphtheriae*. *Infect. Immun.* **59**, 3903–3908.
7. Schmitt, M.P. & Holmes, R.K. (1991). Iron-dependent regulation of diphtheria toxin and siderophore expression by the cloned *Corynebacterium diphtheriae* repressor gene *dtxR* in *C. diphtheriae* C7 strains. *Infect. Immun.* **59**,1899–1904.
8. Tao, X., Boyd, J. & Murphy, J.R. (1992). Specific binding of the diphtheria tox regulatory element DtxR to the *tox* operator requires divalent heavy metal ions and a 9-base-pair interrupted palindromic sequence. *Proc. Natl. Acad. Sci. USA* **89**, 5897–5901.
9. Schmitt, M.P., Twiddy, E.M. & Holmes, R.K. (1992). Purification and characterization of the diphtheria toxin repressor. *Proc. Natl. Acad. Sci. USA* **89**, 7576–7580.
10. Boyd, J.M., Hall, K.C. & Murphy, J.R. (1992). DNA sequences and characterization of *dtxR* alleles from *Corynebacterium diphtheriae* PW8(–), 1030(–) and C7hm723(–). *J. Bacteriol.* **174**, 1268–1272.
11. Krafft, A.E., Tai, S.P., Coker, C. & Holmes, R.K. (1992). Transcription analysis and nucleotide sequence of *tox* promoter/operator mutants of corynebacteriophage beta. *Microb. Pathog.* **13**, 85–92.
12. Tao, X. & Murphy, J.R. (1993). Cysteine-102 is positioned in the metal binding activation site of the *Corynebacterium diphtheriae* regulatory element DtxR. *Proc. Natl. Acad. Sci. USA* **90**, 8524–8528.
13. Schmitt, M.P. & Holmes, R.K. (1994). Cloning, sequence and footprint analysis of two promotor/operators from *Corynebacterium diphtheria* that are regulated by the diphtheria toxin repressor (DtxR) and iron. *J. Bacteriol.* **176**, 1141–1149.
14. Schmitt, M.P. & Holmes, R.K. (1993). Analysis of diphtheria toxin repressor–operator interactions and characterization of a mutant repressor with decreased binding activity for divalent metals. *Mol. Microbiol.* **9**, 173–181.
15. Tao, X. & Murphy, J.R. (1992). Binding of the metalloregulatory protein DtxR to the diphtheria *tox* operator requires a divalent heavy metal ion and protects the palindromic sequence from DNase I digestion. *J. Biol. Chem.* **267**, 21761–21764.
16. Wang, Z., Schmitt, M.P. & Holmes, R.K. (1994). Characterization of mutations that inactivate the diphtheria toxin repressor gene (*dtxR*). *Infect. Immun.* **62**, 1600–1608.
17. Holmes, R.K. & Schmitt, M.P. (1994). Bacteriophages — bacterial toxins. In *Encyclopedia of Virology*. (Webster, R.G. & Granoff, A., eds), pp. 101–106, Academic Press, London.
18. Schultz, S.C., Shields, G.C. & Steitz, T.A. (1991). Crystal structure of a CAP–DNA complex: the DNA is bent by 90°. *Science* **253**, 1001–1007.
19. Ramakrishnan,V., Finch, J.T., Graziano, V., Lee, P.L. & Sweet, R.M. (1993). Crystal structure of globular domain of histone H5 and its implications for nucleosome binding. *Nature* **362**, 219–223.
20. Clarke, N.D., Beamer, L., Goldberg, H.R., Berkower, C. & Pabo, C.O. (1991). The DNA binding arm of λ repressor: critical contacts from a flexible region. *Science* **254**, 267–270.
21. Steitz, T.A. (1990). Structure studies of protein–nucleic acid interaction: the source of sequence-specific binding. *Q. Rev. Biophys.* **23**, 205–280.
22. Nicholls, A. & Honig, B. GRASP. Columbia University, New York.
23 McKay, D.B. & Steitz, T.A. (1981). Structure of catabolite gene activator protein at 2.9 Å resolution suggests binding to left-handed B-DNA. *Nature* **290**, 744–749.
24. Wolberger, C., Dong, Y., Ptashne, M. & Harrison, S.C. (1988). Structure of a phage 434 Cro/DNA complex. *Nature* **335**, 789–795.
25. Otwinowski, Z., *et al.*, & Sigler, P.B. (1988). Crystal structure of trp repressor/operator complex at atomic resolution. *Nature* **35**, 321–329.
26. Howard, A.J., Gilliland, G.L., Finzel, B.C., Poulos, T.L., Olhendorf, D.H. & Salemme, F.R. (1987). The use of an imaging proportional counter in macromolecular crystallography. *J. Appl. Crystallogr.* **20**, 383–387.
27. Leslie, A.G.W. (1992). In *Joint CCP4 and ESF-EACMB Newsletter on Protein Crystallography*, No.26. Daresbury Laboratory, Warrington, UK.
28. Collaborative Computational Project, Number 4 (1994). The CCP4 suite: programs for protein crystallography. *Acta Crystallogr. D* **50**, 760–763.
29. Otwinowski, Z. (1991). Maximum likelihood refinement of heavy atom parameters. In *Isomorphous Replacement and Anomalous Scattering*. pp. 80–86. Daresbury Laboratory, Warrington, UK.
30. Jones, T.A., Zou, J Y., Cowan, S.W. & Kjeldgaard, M. (1991). Improved methods for building protein models in electron density maps and the location of errors in these models. *Acta Crystallogr. A* **47**,110–119.
31. Brünger, A.T., Kuriyan, J. & Karplus, M. (1987). Crystallographic R factor refinement by molecular dynamics. *Science* **235**, 458–460.
32. Laskowski, R.A., MacArthur, M.W., Morris, A.L. & Thornton, J.M. (1993). PROCHECK: a program to check the stereochemical quality of protein structures. *J. Appl. Crystallogr.* **26**, 283–291.
33. Kraulis, P.J. (1991). MOLSCRIPT: a program to produce both detailed and schematic plots of protein structures. *J. Appl. Crystallogr.* **24**, 946–950.
34. Bacon, D.J. & Anderson, W.F. (1988). A fast algorithm for rendering space-filling molecule pictures. *J. Mol. Graphics* **6**, 219–220.
35. Merritt, E.A. & Murphy, M.E.P. (1994). Raster 3D version 2.0: A program for photorealistic molecular graphics. *Acta Crystallogr. D* **50**, 869–873.

Received: **24 Oct 1994**; revisions requested: **2 Nov 1994**; revisions received: **16 Nov 1994**. Accepted: **25 Nov 1994**.